For publication in *Chemosphere*

Why is Calcite a Strong Phosphorus Sink in Freshwater? Investigating the Adsorption Mechanism Using Batch Experiments and Surface Complexation Modeling

Hilary Flower, Mark Rains, Yasemin Taşcı[1], Jia-Zhong Zhang, Kenneth Trout, David Lewis, Arundhati Das, Robert Dalton

Dr. H. Flower (corresponding author)
Eckerd College, 4200 54th Ave S, St. Petersburg, Florida, 33711, United States
E-mail: flowerhd@eckerd.edu
Phone: (
Fax: (727) 864-8382

Dr. H. Flower, Dr. M. Rains, Y. Taşcı[1], Dr. K. Trout, A. Das, R. Dalton
School of Geosciences, University of South Florida, 4202 E. Fowler Ave, Tampa, Florida, 33620, United States

Dr. J.-Z. Zhang
Ocean Chemistry and Ecosystems Division, Atlantic Oceanographic and Meteorological Laboratory, National Oceanic and Atmospheric Administration, Miami, Florida 33149, United States

Dr. D. Lewis
Department of Integrative Biology, University of South Florida, 4202 E. Fowler Ave, Tampa, Florida, 33620, United States

A. Das
Chemical Engineering, University of South Florida, 4202 E. Fowler Ave, Tampa, Florida, 33620, United States

[1] Current address for Yasemin Taşcı:

Abstract

One of the primary drivers of Phosphorus (P) limitation in aquatic systems is P adsorption to sediments. Sediments adsorb more P in freshwater compared to other natural solutions, but the mechanism driving this difference is poorly understood. To provide insights into the mechanism, we conducted batch experiments of P adsorption to calcite in freshwater and seawater, and used computer software to develop complexation models. Our simulations

revealed three main reasons that, combining together, may explain the greater P adsorption to calcite in freshwater vs. seawater. First, aqueous speciation of P makes a difference. The ion pair $CaPO_4^-$ is much more abundant in freshwater; although seawater has more Ca^{2+} ions, $MgHPO_4^0$ and $NaHPO_4^0$ are more thermodynamically favored. Second, the adsorbing species of P make a difference. The ion pair $CaPO_4^-$ (the preferred adsorbate in freshwater) is able to access adsorption sites that are not available to HPO_4^{2-} (the preferred adsorbate in seawater), thereby raising the maximum concentration of P that can adsorb to the calcite surface in freshwater. Third, water chemistry affects the competition among ions for surface sites. Other ions (including P) compete more effectively against CO_3^{2-} when immersed in freshwater vs. seawater, even when the concentration of HCO_3^-/CO_3^{2-} is higher in freshwater vs. seawater. In addition, we found that under oligotrophic conditions, P adsorption is driven by the higher energy adsorption sites, and by the lower energy sites in eutrophic conditions. This study is the first to model P adsorption mechanisms to calcite in freshwater and seawater.

Keywords

Calcium carbonate, phosphates, abiotic factors, sediment dynamics, nutrient

1. Introduction

Inorganic phosphorus (P) is an essential nutrient in terrestrial and estuarine ecosystems. Any change in P availability is important in aquatic ecosystems because it regulates primary productivity, and if it is in excess it can lead to eutrophication. In a recent global meta-analysis, P limitation of aboveground plant production was much more pervasive than previously thought, comprising nearly half of the 652 natural terrestrial ecosystems studied (Hou et al., 2020).

Because of the sensitivity of terrestrial and coastal ecosystems to P availability, it is important to understand the processes that regulate P fluxes.

Dissolved P enters aquatic systems naturally due to dissolution of phosphate minerals such as apatite, and as a result of human impacts such as soil erosion, deforestation, sewage injection, and the use of fertilizers (Riemersma et al., 2006). Because dissolved P adsorbs strongly to sediment and soil when immersed in freshwater, this depresses dissolved P concentrations in favor of higher particulate P concentrations (Bowes 2003, Owens and Walling 2002). Consequently, adsorption drives P limitation in many terrestrial ecosystems, a process termed "sink-driven P limitation" (Paludan and Morris, 1999; Vitousek et al., 2010). In many freshwater ecosystems, P adsorption to soil reduces eutrophication downstream, and for this reason wetland soil has been harnessed for mitigation purposes (Reddy and Graetz, 1981; Richardson, 1985; Vitousek et al., 2010).

Strong P adsorption to sediments appears to be a feature of immersion in freshwater, as the same is not observed for immersion in seawater (Zhang and Huang, 2011). Because P adsorption is a major driver of P fluxes in freshwater environments, it is important that we understand the mechanism governing it. Unfortunately, we have not as yet established quantitatively the exact chemical reactions that cause P to adsorb to sediment so strongly in freshwater. Understanding these chemical reaction mechanisms would allow us to better predict P availability in both freshwater regions. Filling this knowledge gap becomes more urgent in the face of increasing human perturbation on the P cycle in aquatic environments (Prastka et al., 1998; Filippelli, 2008). Accordingly, the present study aims to answer the question: Why does P adsorb more strongly to calcite when immersed in freshwater vs. seawater?

Previous laboratory experiments can provide valuable clues. In simple CaCO3 and NaCl solutions, the presence of both Ca^{2+} and Mg^{2+} enhances P adsorption, making cooperative adsorption of Ca^{2+}-P and Mg^{2+}-P pairs at the surface of $CaCO_3$ and goethite seem likely (Millero et al., 2001; Gao and Mucci, 2003). However, laboratory experiments cannot test the plausibility of specific alternative chemical reactions, nor test for the effects of single ions in complex electrolyte solutions such as natural freshwater. Geochemical modeling is a tool that uses chemical thermodynamics to investigate plausible chemical reactions to explain field observations. Researchers studying a wide range of adsorbates and adsorbents have used computer programs to develop surface complexation models to explain the adsorption behavior observed in the laboratory and field (Dzombak and Morel, 1990).

To investigate, it was necessary to choose a mineral phase, because the precise chemical reactions of P at the mineral surface depends on the composition of the solid particle. We chose to focus on calcite as the adsorbing surface in the present study because adsorption of P to $CaCO_3$ minerals is thought to be a major control of P concentrations in freshwater settings (Riemersma et al., 2006) and marine settings (de Kanel and Morse, 1978; Morse et al., 1985). Further, many coastal regions are carbonate-based, such as northeast Qatar on the Persian Gulf, the Ryukyus of Japan, the Maltese Islands, Mallorca, Spain, and the Florida Everglades (Shinn, 1973; Zhou and Li, 2001; Kogure et al., 2006; Brandano et al., 2009; Garing et al., 2013). Calcite is the dominant form of calcium carbonate at the Earth's surface (Lee et al., 2016). Yet few studies have considered how the interaction of calcite and seawater affects P adsorption dynamics.

An additional advantage in focusing on calcite is that surface complexation reactions and affinity constants for $CaHPO_4^0$, $CaPO_4^-$, and HPO_4^{2-} are available in the literature to be used as a

106 launchpad for the present study (Sø et al., 2011). These pre-existing models were developed
107 using simple synthetic solutions, and we will adapt them for use with the complex electrolytes of
108 found in natural waters. To probe for the mechanism driving P dynamics of calcite immersed in
109 these complex natural solutions, we combined laboratory experiments and geochemical
110 modeling using geochemical software. We aimed to develop the first (to our knowledge) surface
111 complexation model that can simulate P adsorption to calcite in natural freshwater. A surface
112 complexation model of P dynamics for calcite in freshwater would be useful for projecting P
113 fluxes in field settings.
114

115 ## 2. Experimental Procedures

116 ### 2.1 Calcite

117 We used calcite from ACROS Organics that was reagent-grade (99+% pure). The
118 specific surface area (0.68 m^2 g^{-1}) was measured by N_2 Brunauer–Emmett–Teller (BET).
119

120 ### 2.2 Solutions

121 To better approximate field conditions, we used two natural water types. We used a
122 peristaltic pump to extract fresh groundwater (hereafter referred to as "freshwater") from the
123 carbonate-based Floridan aquifer, from a well on the campus of University of South Florida,
124 Tampa, FL, USA. To compare freshwater to contrasting natural water, we took a sample of
125 seawater from the surface of the Gulf of Mexico near Fort DeSoto Park, St Petersburg, FL, USA.
126 Since natural seawater is supersaturated with respect to calcite, we pre-equilibrated both
127 solutions to calcite at a solid to solution ratio of 2 g L^{-1} overnight and filtered (0.2 μm) following
128 Millero et al. (2001).

We found that even with pre-equilibrating our solutions to calcite as previously described, a subsequent addition of new calcite resulted in a decrease of solution pH, suggesting further calcite precipitation. To identify a calcite equilibrium condition in seawater under ambient atmospheric CO_2 (indoor condition), we approached the system from both ends, dissolution at low pH and precipitation at high pH, to locate a boundary condition where calcite neither dissolves nor precipitates in seawater. We conducted a series of preliminary batch experiments with 1 g calcite and 40 mL seawater (with and without pre-equilibration to calcite), in which we adjusted the initial pH of the solutions to cover a range from 7.0-11.0, equilibrated them overnight to calcite (with and without added P), and then measured the final pH. We found a crossover point at initial pH between 7.6-7.8 in seawater where $\Delta pH \approx 0$ (Figure 1). Thus, to avoid calcite precipitation/dissolution, we used HCl to adjust both freshwater and seawater to pH = 7.7 prior to batch experiments. We also note that pH = 7.7 is ecologically relevant, since it is within the typical range of water in many coastal aquatic systems.

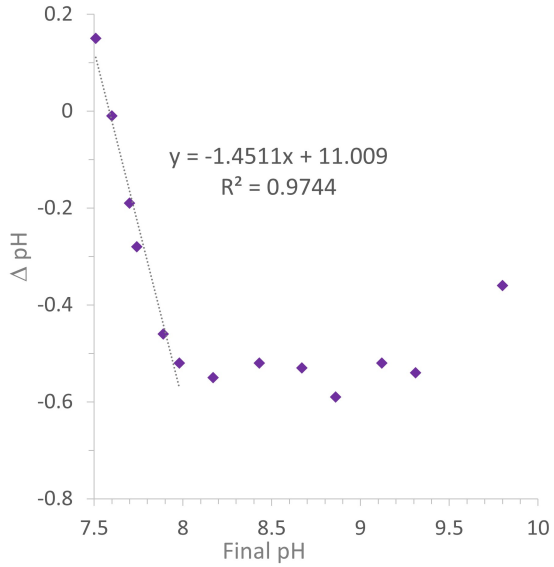

143

144 **Figure 1** Change in pH for seawater (that had previously been equilibrated with calcite and then
145 filtered) that was adjusted to a range of initial pH with HCl, and then exposed to new calcite in a
146 test tube for 24 hours before being measured for final pH ($\Delta pH = pH_{final} - pH_{initial}$).
147

148

149 **2.3 Major ionic components of waters**

150 We measured conductivity and pH using a Thermo Scientific Orion Star A215 Benchtop
151 pH/Conductivity Meter. Solution concentrations of Ca^{2+} and Mg^{2+} were measured by Inductively
152 Coupled Plasma-Atomic Emission Spectrometry. Concentrations of SO_4^{2-} were measured by ion
153 chromatography. We measured P concentrations in the solutions as soluble reactive phosphorus
154 (SRP) by measuring absorbance at 630 nm in 96-well microplates on a BioTek EPOCH
155 microplate spectrophotometer, using the microscale malachite green method (D'Angelo et al.,
156 2001). The key characteristics of our freshwater and seawater (after pre-equilibration to calcite)
157 are listed in Table 1.

158

Table 1: Selected characteristics of the two field waters used in experiments.

Water Type	pH	Salinity psu	Ca^{2+} mM	Mg^{2+} mM	Na^{+} mM	Cl^{-} mM	SO_4^{2-} mM	Total Alkalinity as HCO_3^{-} mM
Freshwater	8.21	0.1	2.75	0.2	0.7	0.8	1.66	2.98
Seawater	8.05	40.0	9.75	49.3	521.1	606.7	10.4	2.43

2.4 Batch Experiments

We studied phosphate adsorption using batch incubation methods adapted from Froelich (1988). We used 1.000 g calcite in 0.040 L solution, a surface to liquid ratio of 37.9 $m^2\ L^{-1}$. Stock solutions of phosphate (1 mM) were prepared with reagent grade Na_2HPO_4. To preserve the pH of our solutions after adding P, we adjusted the stock P solution to pH = 7.7. Phosphate was added to the batches to create 30 increments of initial P concentration ($[SRP]_i$) ranging from 2 µM to 60 µM (Millero et al., 2001). Triplicates were made at 32 µM P to evaluate analytical precision (coefficient of variation was 6.4% for seawater and 1.7% for freshwater). We added chloroform to inhibit microbial activity (Detenbeck and Brezonik, 1991). Tubes were incubated at room temperature on a platform shaker (200 rpm) for 24 hours. Following this, each suspension was filtered using a 0.45 µm nylon syringe filter. An aliquot from each filtrate was then analyzed to measure the final SRP. Any loss of P from the solution under incubation condition is assumed to have been adsorbed to the mineral surface rather than apatite precipitation (see Appendix B for thorough discussion). The amount of P adsorbed on the calcite, ΔP_{ads} (µmol P g^{-1}), is calculated from the difference between initial SRP ($[SRP]_i$) and the final SRP ($[SRP]_f$) concentration, and normalized to 1 g of calcite and 1 L of solution:

$$\Delta P_{ads} = ([SRP]_i - [SRP]_f) \times \frac{0.04\ L\ solution}{1\ g\ calcite} \quad . \qquad [1]$$

where 1.000 g calcite and 40.0 mL solution used in the experiments were taken account in the equation 1.

A plot of ΔP_{ads} vs. $[SRP]_f$ is used to describe the adsorption behavior of P with calcite when immersed in the two water types. The resulting curves are commonly referred to as isotherm curves, emphasizing the temperature dependency of the P adsorption dynamics represented.

2.5 Adsorption Isotherm Parameters

Fitting empirical data to Freundlich Isotherm and Two Surface Langmuir Isotherm equations can provide insights into overall aspects of P adsorption. We used log-weighted error to fit the parameters.

The Langmuir model is a theoretical approach that assumes the solid surface has a finite number of available adsorption sites, with adsorption reaching saturation at a maximum monolayer adsorption capacity or saturation concentration (P_{max}). Such behavior can be modeled as:

$$\Delta P_{ads} = \frac{K_{eq} P_{max} [SRP]_f}{(1 + K_{eq} [SRP]_f)} \quad . \qquad [2]$$

where the constant K_{eq} (μM^{-1}) is related to the binding energy of the adsorption sites on the solid surface, and has also been described as the affinity of P for the surface in the given solution.

Equation [2] assumes that all adsorption sites on the surface have uniform bonding energies, but the surfaces of most solids are heterogeneous. Syers et al. (1973) and Fetter (1977) developed a test: in a plot of $[SRP]_f / \Delta P_{ads}$ vs. $[SRP]_f$, one line segment indicates one surface, and two line segments indicate two surfaces. The Langmuir Two-Surface Sorption Isotherm is written (Langmuir, 1918):

200 $$\Delta P_{ads} = \frac{K_{eq1} P_{max1} [SRP]_f}{(1+K_{eq1}[SRP]_f)} + \frac{K_{eq2} P_{max2} [SRP]_f}{(1+K_{eq2}[SRP]_f)} \quad [3]$$

201 where the Langmuir model of adsorption for a single surface (equation 2) is expanded to
202 accommodate adsorption at two surfaces (Holford et al., 1974). The two "surfaces" represent two
203 types of adsorption site at the interface between the solid and aqueous phase (the physical
204 differences between these two types of sites on the crystal lattice are explored further in section
205 5.1.). The first quantity on the product side represents the surface with the higher bonding
206 energy, and each of the parameters in equation 1 are appended with the subscript 1. The second
207 quantity (with subscript 2) represents the lower bond energy. In this model, P ions adsorb to both
208 types of sites throughout the incubation, in proportion to the bonding energy of the unoccupied
209 sites (Holford et al., 1974).

210 The Freundlich isotherm model is an empirical approach particularly suited to
211 heterogeneous surfaces such as soils and minerals (Freundlich, 1906). The Freundlich Isotherm
212 equation is given as:

213 $$\Delta P_{ads} = (K_f \times [SRP]_f^n) \quad . \quad [4]$$

214 The Freundlich exponent, n, accounts for the heterogeneity of the solid surface; it is a number
215 between 0 and 1. The lower the exponent, the more pronounced is the flattening of the isotherm
216 curve, i.e., a higher contrast between intense (steep) P adsorption initially (at a higher energy
217 surface), followed by weak adsorption as those more limited sites become filled, and a greater
218 proportion of adsorption occurs at lower energy sites (which flattens the curve). As n approaches
219 1, P adsorption approaches linearity (no difference between high and low energy sites). The
220 Freundlich coefficient (K_f) is the relative adsorption capacity, or the relative rate of removal of

phosphorus per unit increase in $[SRP]_i$ (Yakubu et al., 2008). The Freundlich coefficient (K_f) functions as a scalar of total adsorption, with higher coefficient values resulting in higher total P adsorption (ΔP_{ads}).

2.6 Computer modeling approach

2.6.1 Geochemical software

We used the geochemical modeling program PHREEQC (Version 3.6) (Parkhurst and Appelo, 1999; Parkhurst and Appelo, 2013). This program was developed by the United States Geological Survey (USGS) to simulate a broad range of aqueous geochemical batch-interactions including aqueous speciation, saturation index, dissolution/precipitation, and surface complexation. The program uses a thermodynamic database consisting of a wide range of data for equilibria among aqueous complexes and the solubility of solid phases, and it uses these to predict geochemical outcomes at equilibrium. The user can make any changes or additions to the thermodynamic data used for the simulations. We wrote code to simulate the procedures for our freshwater and seawater batch experiments (described in Section 2.4; full codes are provided in Appendix A), and made additions and adjustments to the thermodynamic database (described below in Sections 2.6.2-2.6.4). Output collected from PHREEQC included the predicted ΔP_{ads}, the distribution of surface complexes, the distribution of aqueous species, and the saturation index of apatite.

2.6.2 Equilibria at the surface of calcite

Surface complexation models (SCMs) are a quantitative thermodynamic approach that simulate chemical equilibria at the interface between a mineral and its surrounding solution.

244 These chemical models account for the effects of variable chemical conditions and allow the user
245 to compare the plausibility of alternative reactions (Goldberg et al., 2007). In SCMs, adsorption
246 reactions are defined and given specific equilibrium (stability or affinity) constants, analogous to
247 aqueous complexes in the bulk solution. The surface reactions also determine the charge at the
248 mineral surface, which in turn affects adsorption reactions.
249 Various SCMs differ in how they conceptualize and quantify the electrical charge
250 distribution between the mineral surface and the bulk solution. We used the Constant
251 Capacitance Model (CCM), a quantitative approach to surface interactions that is thought to be
252 particularly well-suited to modeling high ionic strength solutions such as seawater (Gao and
253 Mucci, 2003). It also performs better for heterogeneous surfaces than some other models, such as
254 CD-MUSIC (Zhou et al., 2005). Sø et al. (2011) presented an adjustment to PHREEQC code to
255 approximate the CCM. As a starting point for our model, we used previous CCM models for
256 adsorption to carbonates started by Van Cappellen et al. (1993), and further developed by
257 Pokrovsky et al. (2000), Pokrovsky and Schott (2002), Hiorth et al. (2010), and Sø et al. (2011)
258 (Table 2). The primary sites at the calcite surface are calcium (denoted as $>Ca^{+}$) and carbonate
259 functional groups ($>CO_3^{-}$) in equal abundance (where the symbol > is used to denote the polar
260 $CaCO_3$ surface with a terminal Ca^{+} or CO_3^{-}, being charge-balanced by the opposite end of the
261 same $CaCO_3$ molecule in the crystal lattice). Calcium sites are broken into strong sites (denoted
262 as $>sCa^{+}$) and weak sites ($>wCa^{+}$), and P adsorbs to these sites as $CaPO_4^{-}$, $CaHPO_4^{0}$, or HPO_4^{2-}
263 in competition with CO_3^{2-}, HCO_3^{-}, SO_4^{2-}, and H_2O^{0} in solution (Table 2). In addition, Ca^{2+}, Mg^{2+}
264 and H^{+} compete for the carbonate group adsorption sites ($>CO_3^{-}$). and at both strong and weak
265 calcium adsorption sites, P (as $CaPO_4^{-}$ and either $CaHPO_4^{0}$, or HPO_4^{2}) competes with CO_3^{2-},
266 HCO_3^{-}, SO_4^{2-}, and H_2O (Figure 2). We also tested a model that included cooperative adsorption

between Mg^{2+}–P ion pairs and the surface, substituting Mg^{2+} for Ca^{2+} in the surface complexation models in the lower two sections of Table 2 as a starting point.

One of the parameters that must be set is the ratio of strong to weak sites. According to Dzombak and Morel (1990), strong sites typically have lower density than weak sites. We adopted the total site density of 8.22 μmol /m^2 for both calcium and carbonate sites, and the ratio of strong:weak sites from Pokrovsky and Schott (2002) and Sø et al. (2011). The ratio of strong vs. weak sites determines the curvature of the isotherms; the fact that our modeled curves matched well with our experimental results suggests that this assumption was acceptable in this study.

Table 2 Summary of surface complexation reactions and associated affinity constants from published literature[a,b,c] for negatively charged sites ending with a carbonate group (>CO_3^-), strong positively charged sites (>sCa^+) and weak positively charged sites (>wCa^+) at the surface of calcite. The error interval corresponds to the 95% confidence level. Phosphate reactions with the calcite surface are listed as two alternative models in the bottom two sections, each consisting of four reactions, as developed by Sø et al. (2011) for calcite in calcium carbonate solutions.

Reaction	**Log K**
$>CO_3H = >CO_3^- + H^+$	-5.1 ± 0.03[a]
$>CO_3H + Ca^{2+} = >CO_3Ca^+ + H^+$	-1.7 ± 0.06[a]
$>CO_3H + Mg^{2+} = >CO_3Mg^+ + H^+$	-1.7 ± 0.06 [a]
$>sCaCO_3^- + H_2O = >sCaOH_2^+ + CO_3^{2-}$	-5.25 ± 0.03[a]
$>wCaCO_3^- + H_2O = >wCaOH_2^+ + CO_3^{2-}$	-5.25 ± 0.03
$>sCaCO_3^- + HCO_3^- = >sCaHCO_3 + CO_3^{2-}$	-3.929 ± 0.06[a]
$>wCaCO_3^- + HCO_3^- = >wCaHCO_3 + CO_3^{2-}$	-3.929 ± 0.06
$>sCaCO_3^- + SO_4^{2-} = >sCaSO_4 + CO_3^{2-}$	-3.15[b]
$>wCaCO_3^- + SO_4^{2-} = >wCaSO_4 + CO_3^{2-}$	-3.15
Model 1 from Sø et al. (2011)	0.90 ± 0.06[c]
$>sCaCO_3^- + CaHPO_4^0 = >sCaHPO_4Ca^+ + CO_3^{2-}$	
$>wCaCO_3^- + CaHPO_4^0 = >wCaHPO_4Ca^+ + CO_3^{2-}$	-1.75 ± 0.07
$>sCaCO_3^- + CaPO_4^- = >sCaPO_4Ca^0 + CO_3^{2-}$	2.21 ± 0.03
$>wCaCO_3^- + CaPO_4^- = >wCaPO_4Ca^0 + CO_3^{2-}$	-0.79 ± 0.07
Model 2 from Sø et al. (2011)	0.17 ± 0.16[c]
$>sCaCO_3^- + HPO_4^{2-} = >sCaHPO_4^- + CO_3^{2-}$	

$>wCaCO_3^- + HPO_4^{2-} = >wCaHPO_4^- + CO_3^{2-}$	-2.00 ± 0.15
$>sCaCO_3^- + CaPO_4^- = >sCaPO_4Ca^0 + CO_3^{2-}$	2.30 ± 0.05
$>wCaCO_3^- + CaPO_4^- = >wCaPO_4Ca^0 + CO_3^{2-}$	-0.72 ± 0.10

[a] Pokrovsky and Schott (2002)
[b] Hiorth et al. (2010)
[c] Sø et al. (2011)

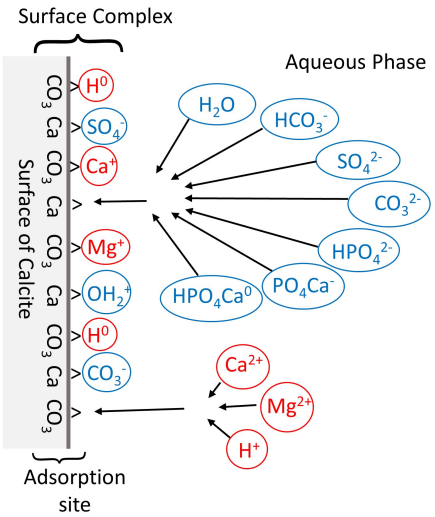

300 **Figure 2** Simplified, schematic representation of surface complexes at the calcite/water interface
301 at positive $>Ca^+$ and negative $>CO_3^-$ sites, partially based on illustrations by Gao and Mucci
302 (2003) and Mahani et al. (2017).
303

304

305 Our efforts for the present study were directed at determining which of the previously
306 published surface complexation reactions (Table 2) were necessary to reproduce our
307 experimental data for the two water types, and to assign affinity constants to the selected P
308 sorption reactions, specific to the water type. It is not possible to directly use previously
309 published reactions and affinity constants to simulate reactions in freshwater and seawater,
310 because affinity constants are specific to the physico-chemical characteristics of the mineral
311 phase, solutions, and conditions of the experiments from which they were derived. Affinity
312 constants developed in single or dual electrolyte solutions do not account for the competition that
313 occurs in more complex solutions (Sø et al., 2008). No surface complexes or affinity constants
314 have been developed for calcite or any mineral in seawater. The interdependency of the many
315 adsorbing species make it impossible to calibrate surface complexes for several adsorbing
316 species at once. To narrow down P surface reactions and to calibrate associated affinity
317 constants, we used PEST (version 16.0), a computer program that offers model-independent
318 parameter estimation and uncertainty analysis developed by Doherty (2004).
319

320 ***2.6.3 Calcite solubility***

321 Calcite is more soluble in seawater than in pure water, and this must be taken into
322 account when dissolution/precipitation of calcite is an important part of an experiment. For our
323 freshwater experiments, we used the intrinsic calcite solubility (K_{sp}= -8.48) (Langmuir, 1968;

Plummer and Busenberg, 1982). For our seawater experiments, we used the apparent solubility of calcite in seawater at 25 °C and 1 atmosphere of pressure (K_{sp}*= -6.35) (Morse et al., 1980).

2.6.4 Equilibria in solution

To model aqueous speciation in our freshwater solution, we used intrinsic association constants (K_{int}, from the database phreeqc.dat) (Table 3). We compared results with the phreeqc.dat database and another database (wateq.v4), and found no difference in predicted ΔP_{ads}. To model aqueous speciation in our seawater solution, we used apparent affinity constants for seawater at 25 °C (K*) (Table 3).

Table 3 Stoichiometric aqueous complexation constants for K_{int} (from PHREEQC.dat database) and K* for seawater (25°C) from the published literature[b, c]

Reactions	Log K_{int}	Seawater Log K*
$H_2O = OH^- + H^+$		-13.215[b]
$CO_3^{2-} + H^+ = HCO_3^-$	10.329[a]	8.95[b]
$PO_4^{3-} + H^+ = HPO_4^{2-}$	12.34[a]	21.721[b]
$PO_4^{3-} + 2H^+ = H_2PO_4^-$	19.553[a]	19.76[b]
$PO_4^{3-} + 3H^+ = H_3PO_4^0$	21.721[a]	16.337[b]
$Na^+ + HPO_4^{2-} = NaHPO_4^-$	0.29[a]	0.05[c]
$Na^+ + H_2PO_4^- = NaH_2PO_4$	absent	-0.54[c]
$Na^+ + PO_4^{3-} = NaPO_4^{2-}$	absent	0.52[c]
$Mg^{2+} + SO_4^{2-} = MgSO_4$	2.37[a]	1.01[c]
$Mg^{2+} + H^+ + CO_3^{2-} = MgHCO_3^+$	11.399[a]	0.28[c]
$Mg^{2+} + CO_3^{2-} = MgCO_3$	2.98[a]	1.94[c]
$Mg^{2+} + H_2O = MgOH^+ + H^+$	-11.44[a]	-12.02[c]
$SO_4^{2-} + H^+ = HSO_4^-$	1.98[a]	1.49[c]
$Ca^{2+} + H_2O = CaOH^+ + H^+$	-12.7[a]	-12.98[c]
$Ca^{2+} + CO_3^{2-} = CaCO_3$	3.224[a]	2.1[c]
$Ca^{2+} + CO_3^{2-} + H^+ = CaHCO_3^+$	11.435[a]	0.33[c]
$Ca^{2+} + SO_4^{2-} = CaSO_4$	2.25[a]	1.03[c]
$Mg^{2+} + PO_4^{3-} = MgPO_4^-$	6.589[a]	3.84[c]
$Mg^{2+} + HPO_4^{2-} = MgHPO_4^0$	2.87[a]	1.51[c]
$Mg^{2+} + H_2PO_4^- = MgH_2PO_4^+$	1.513[a]	0.47[c]
$Ca^{2+} + PO_4^{3-} = CaPO_4^-$	6.45[a]	4.5[c]
$Ca^{2+} + HPO_4^{2-} = CaHPO_4^0$	2.739[a]	1.28[c]

$Ca^{2+} + H_2PO_4^- = CaH_2PO_4^+$	1.408[a]	0.24[c]

[a] From PHREEQC.dat database
[b] From Pierrot and Millero (2016)
[c] Millero and Schreiber (1982)

3. Experimental Results and Isotherm Parameters

Our results showed that P adsorbed more to calcite in freshwater compared with seawater (Figure 3a, Table 4; raw data is provided in Appendix A). The mean ΔP_{ads} in freshwater was 0.84 μmol P g^{-1}, compared to 0.59 μmol P g^{-1} in seawater. Based on our Freundlich Isotherm parameters, freshwater adsorption efficiency was 50% higher than seawater (Freshwater K_f = 0.45 L g^{-1} and Seawater K_f = 0.30 L g^{-1}; Table 4). The dimensionless Freundlich coefficient n was also much higher in freshwater (3.4) compared to seawater (2.8).

Our experimental data could best be represented as having two types of P adsorption sites with contrasting bonding energies (strong and weak). First, when plotted as $[SRP]_f / \Delta P_{ads}$ vs. $[SRP]_f$, the data for both water types exhibited two linear line segments, with the distinction being more pronounced in freshwater (Figure 3b). Fitting the data for both water types to Equation 2 did not work well ($R^2 < 0.86$), the fit was much better ($R^2 \geq 0.96$) using the Langmuir Two-Surface Sorption Isotherm (Equation 3). Two surfaces were sufficient to explain our empirical data with the minimal number of parameters.

The saturation concentrations for both surfaces are much higher in freshwater than seawater (freshwater's P_{max1} of 0.68 μmol P g^{-1} is 2.8 times higher than seawater's P_{max1} of 0.24 μmol P g^{-1}, and freshwater's P_{max2} of 3.54 μmol P g^{-1} is 4.6 times higher than seawater's P_{max2} of 0.77 μmol P g^{-1}). The k_{eq1} for seawater ten times higher (20.50 μM^{-1}) compared to freshwater (2.13 μM^{-1}). This may be an artifact of our experimental conditions, since this parameter is

359 sensitive to the $[SRP]_f$ measurements of the first few low $[SRP]_f$ data points, which were very
360 close to our detection limit. However, the k_{eq2} is also higher for seawater (0.08 μM^{-1}) compared
361 to freshwater (0.01 μM^{-1}).

362

363 **Table 4: Phosphorus sorption characteristics for calcite with respect to the two water types**

Water type	Freundlich Parameters			Two-Surface Langmuir Parameters				
	K_f , L g^{-1}	n	R^2	P_{max1} µmol P g^{-1}	K_{eq1} μM^{-1}	P_{max2} µmol P g^{-1}	K_{eq2} μM^{-1}	R^2

364 K_f Freundlich adsorption coefficient
365 n Freundlich exponent, dimensionlessP_{max1} Adsorption maximum for the first surface sites
366 K_{eq1} Adsorption energy for the first surface sites
367 P_{max2} Adsorption maximum for the second surface sites
368 K_{eq2} Adsorption energy for the second surface sites
369
370

a)

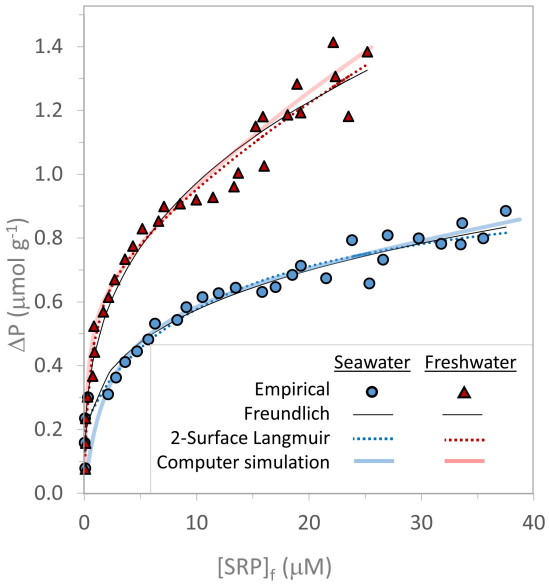

b)

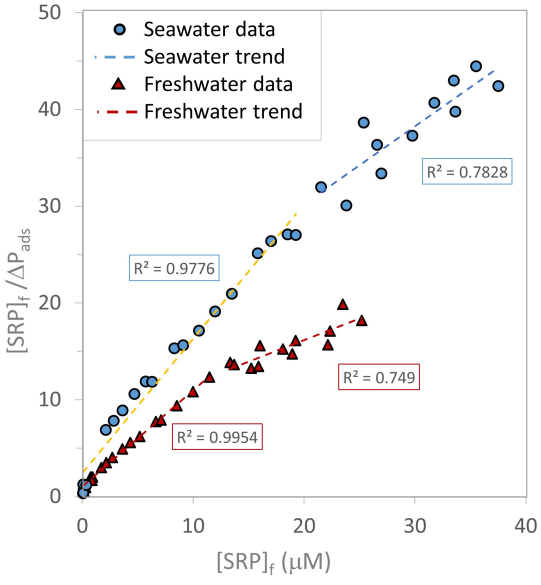

371

Figure 3 Adsorption Isotherm Results a) comparison among freshwater empirical results (black plus symbols), Freundlich Isotherm (thin black curve), Two-Surface Langmuir Isotherm (dotted red curve), and our computer simulation (solid pale red curve; discussed in Section 4.5 below); and the similar for seawater: seawater empirical results (green "x" symbols), Freundlich Isotherm (thin black curve), Two-Surface Langmuir Isotherm (dotted blue curve), and our computer simulation (solid pale blue curve); b) The linear plot of empirical data used to test whether there was more than one type of adsorption site.

4. Modeling Results

4.1 Simulation of P dynamics

We developed models that quite closely matched our empirical ΔP_{ads} in seawater (R^2 = 0.9973) and freshwater (R^2 = 0.9899), as shown in Figure 3a, and Figure 4. For both water types, our best fits were obtained using only a single P species reacting with strong and weak calcium sites: $CaPO_4^-$ for freshwater and HPO_4^{2-} for seawater (Table 5). Inclusion of reactions for Mg^{2+}–P adsorbing at the calcite surface made no difference in total ΔP_{ads} predicted by our models. To see the effect of water type on the viability of the P adsorption reactions, we ran a simulation for the seawater solution but using the P adsorption reactions and Log K values calibrated for freshwater, and the predicted ΔP_{ads} was close to zero (not shown).

Table 5 Our association constants for surface complexation reactions between P species and two kinds of positive sites (Ca) on the $CaCO_3$ surface. The error interval corresponds to the 95% confidence level.

Freshwater (R^2 = 0.9899)	**Log K**
$>sCaCO_3^- + CaPO_4^- = >sCaPO_4Ca^0 + CO_3^{2-}$	3.31 ± 0.33
$>wCaCO_3^- + CaPO_4^- = >wCaPO_4Ca^0 + CO_3^{2-}$	0.72 ± 0.02
Seawater (R^2 = 0.9973)	**Log K**
$>sCaCO_3^- + HPO_4^{2-} = >sCaHPO_4^- + CO_3^{2-}$	1.98 ± 0.08
$>wCaCO_3^- + HPO_4^{2-} = >wCaHPO_4^- + CO_3^{2-}$	-0.51 ± 0.03
Number of carbonate sites $>CO_3^-$ (μmol m^{-2})	8.22
Number of strong calcium sites $>sCa^+$ (μmol m^{-2})	7.31
Number of weak calcium sites $>wCa^+$ (μmol m^2)	0.91

For seawater, our computer model predicted a less steep initial increase than the two isotherms (the steepness of the first five seawater data points was noted as a possible experimental artifact in Section 3), and a slightly greater ΔP_{ads} at high $[SRP]_f$. For freshwater, our computer model predicted slightly more ΔP_{ads} than the two isotherms, particularly at high $[SRP]_f$ (Figure 3a).

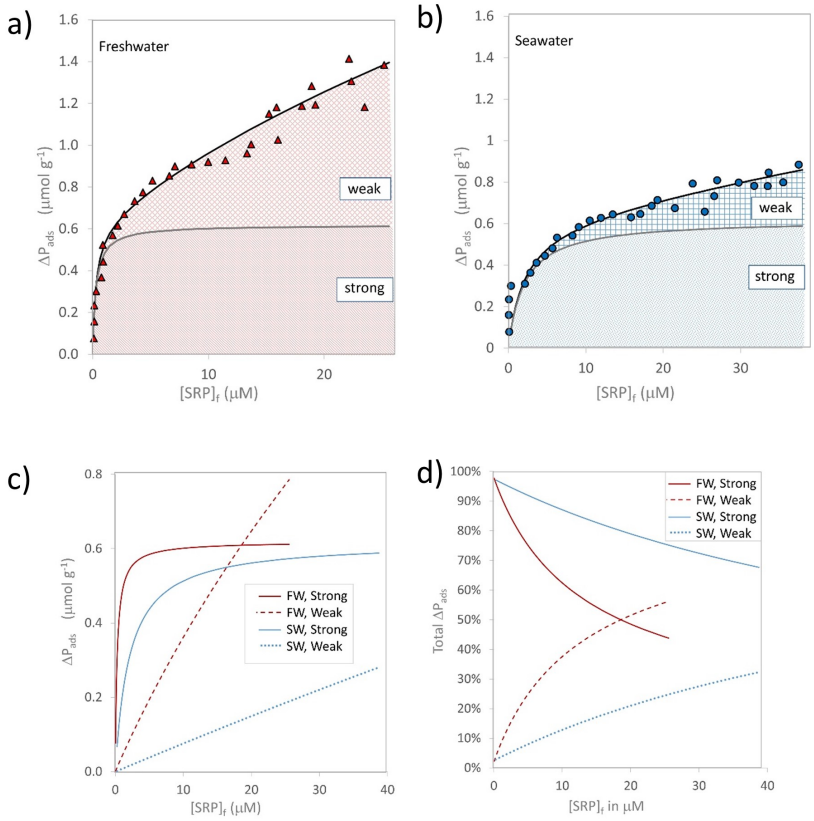

Figure 4 Strong vs. weak calcium sites on the calcite surface for $CaPO_4^-$ in freshwater and HPO_4^{2-} in seawater; in the top row strong vs. weak calcium sites are indicated by shading and are shown additively, with total adsorbed P as a black curve, and empirical results shown as markers for a) freshwater (red triangles) and b) seawater (blue circles); in the bottom row the individual amount of P adsorption at strong (solid curves) vs. weak (dashed curves) is shown for freshwater (red) and seawater (blue), as an absolute concentration (c) and as a proportion of total P adsorbed (d).

4.2 Strong vs. weak calcium sites

Figure 4 shows the relative proportion of P adsorption to strong and weak calcium sites for the two water types in our computer simulations. At $[SRP]_f < 1\mu M$, almost all of the ΔP_{ads} was to strong calcium sites. As $[SRP]_f$ increased ($[SRP]_f \approx 1$ μM for freshwater, and $[SRP]_f \approx 5$ μM for seawater) the strong calcium sites approached saturation and P adsorption to calcite in seawater catches up, ending with only 4% more in freshwater ($\Delta P_{ads} = 0.612$ μmol P g^{-1} in freshwater vs. 0.588 μmol P g^{-1} in seawater; Figure 4c). Meanwhile, P adsorption to the weak calcium sites continued to increase in a linear fashion (Figure 4c). For most of the isotherm curve ($[SRP]_i \approx$ 5-60 μM) the steeper slope of P adsorption to the weak sites in freshwater vs. seawater drives the difference in total P adsorption between the two water types. For freshwater, P adsorption to weak calcium sites comes to exceed P adsorption to strong calcium sites starting at $[SRP]_f > 19$ μM, whereas in seawater P adsorption to weak calcium sites never exceeds 32% of total P adsorbed.

4.3 Distribution of surface sites

We evaluated the proportion of all surface complexes at strong and weak calcium sites, as well as at negative (carbonate) sites on the calcite surface, using $[SRP]_i = 60$ μM for comparison (Figure 5). On strong calcium sites, P overwhelmingly dominates the surface in both Freshwater (99.5%), and seawater (95%). In freshwater, CO_3^{2-} adsorption to strong calcium sites is negligible (0.08%), whereas it is 4.5% of adsorption to strong calcium sites in seawater. In contrast, P occupies a minority of weak calcium sites in both freshwater (16%), and seawater (6%). Adsorption of CO_3^{2-} is much lower in freshwater compared to at both strong calcium sites (0.08% in freshwater, 4.5% in seawater) and weak calcium sites (13% in freshwater, 82% in seawater). More SO_4^{2-} adsorbs to weak sites in freshwater (17%) vs. seawater (2%). Adsorption

of HCO_3^- is negligible for both site types and both water types, only reaching 1% of weak calcium sites in freshwater. At carbonate sites in freshwater, most were occupied by Ca^{2+} (45%) or unoccupied (49%), with a small amount of Mg^{2+} (6%). In seawater, Mg^{2+} dominated (76%), with the remainder being Ca^{2+} (21%) or unoccupied (3%).

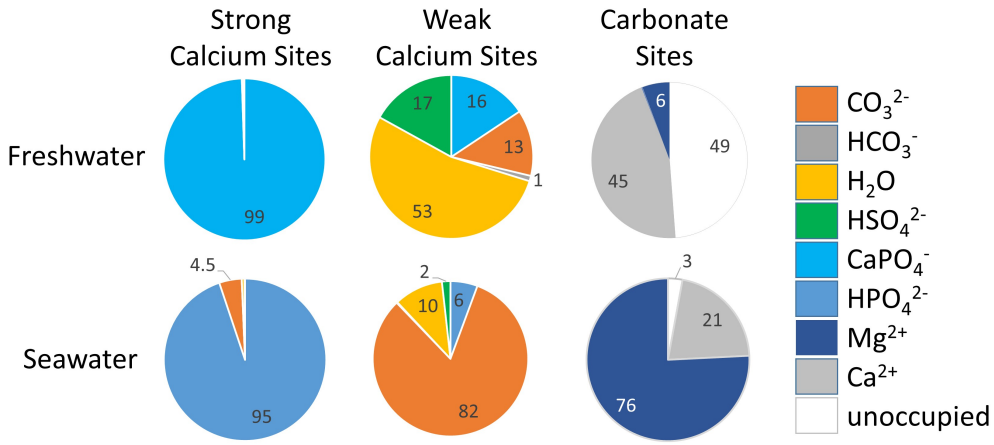

Figure 5 The distribution of surface complexes by water type (freshwater top row, seawater bottom row) and strong calcium sites (left hand column), weak calcium sites (center column), and carbonate sites (right hand column).

We simulated a series of scenarios in PHREEQC to try to better understand the importance of certain ions in solution and their interactions with the surface. We found including surface reactions for SO_4^{2-}, Mg^{2+}, and Ca^{2+} made little difference in the predicted ΔP_{ads} (Figure 6a; for reactions, see Appendix A). Specifically, omission of the SO_4^{2-} reactions produced less than 1% difference in ΔP_{ads}, and a slightly better fit to the experimental data ($R^2 = 0.9968$ without them, $R^2 = 0.9826$ with them).

The omission of Ca^{2+} surface complexes caused a slight over-prediction of ΔP_{ads} (up to 3% at high P doses). The omission of the Mg^{2+} reactions produced up to 0.5% difference in

449 ΔP_{ads}. Because the CO_3^{2-} surface complex is necessary in our script for P to adsorb, it was not

450 possible to omit that complex from our simulations.

451

452

453

454 a)

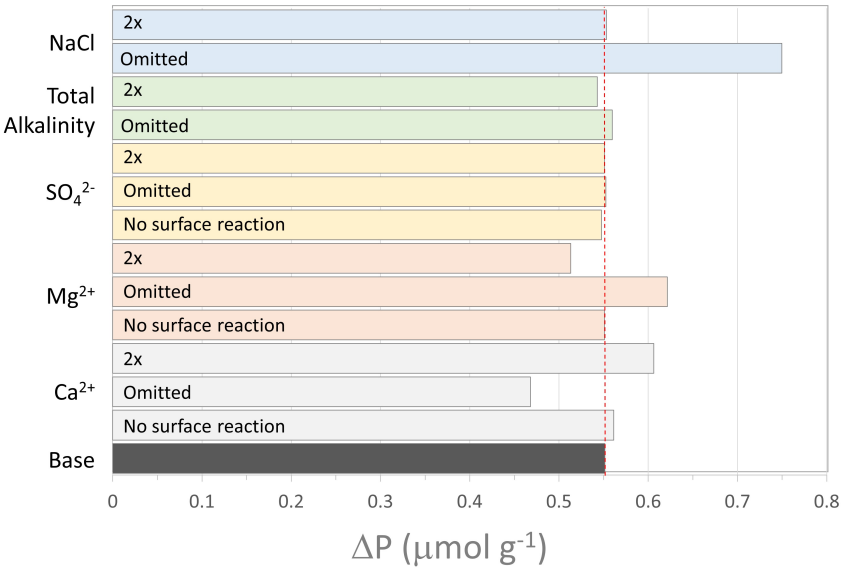

455

456 b)

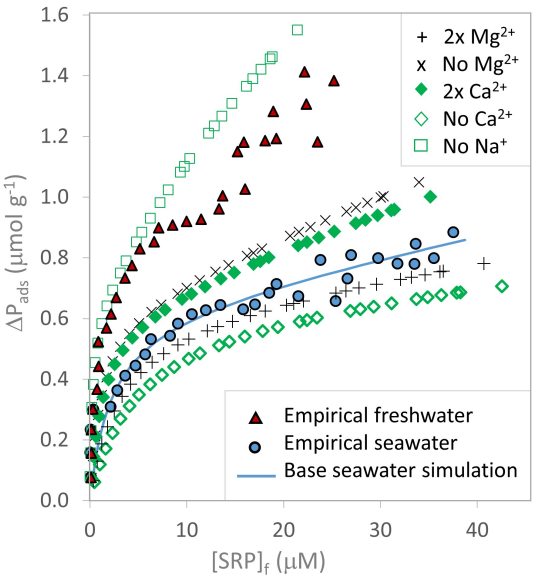

457

458 **Figure 6** The effect of various changes in our PHREEQC code on simulated ΔP_{ads}, compared to
459 our empirical results (blue circles) and seawater model (solid blue curve), for a) various
460 alterations of initial seawater composition and surface reactions on ΔP_{ads} for $[SRP]_i$ = 24 μM; b)
461 the full simulated isotherms for doubling or omitting Mg^{2+} or Ca^{2+} from the initial seawater
462 solution.
463

464 ***4.4 The role of aqueous species***

465 Even without adsorbing to the surface, the presence of certain ions in solution can make a
466 difference in P adsorption, due to changes in aqueous speciation. To explore the influence of
467 solution composition on aqueous speciation and P adsorption, we ran simulations in which we
468 doubled or omitted key ions from the seawater script (Figure 6a and b). As with our changes in
469 surface reactions, the differences were more pronounced at high $[SRP]_f$. Omitting NaCl
470 increased the ΔP_{ads} by up to 81%, exceeding our freshwater empirical data. Doubling NaCl
471 concentration had no effect. The effects of Mg^{2+} and Ca^{2+} ions were nearly mirror images of each
472 other. Omitting Mg^{2+} ions increased ΔP_{ads} by up to 22%, and doubling Mg^{2+} concentration
473 decreased ΔP_{ads} by up to 9%. Conversely, omitting Ca^{2+} ions decreased the ΔP_{ads} by up to 22%,

and doubling Ca^{2+} concentration increased ΔP_{ads} by 16%. The omission of sulfate ions from the initial seawater solution resulted in almost no difference in simulated ΔP_{ads} ($\leq 0.5\%$). The omission of total alkalinity (which mainly consists of $[HCO_3^-] + 2[CO_3^{2-}]$) from the initial seawater solution slightly over-predicted ΔP_{ads} ($\leq 2\%$), and doubling its value slightly under-predicted ΔP_{ads} ($\leq 2\%$).

Speciation of dissolved P species changes with elemental composition of solutions and thus can also make a difference in P adsorption. When compared to the distribution of P species in freshwater (Figure 7a), our seawater (and standard seawater) had more HPO_4^{2-}, $NaHPO_4^0$ and $MgHPO_4^0$, and less $CaHPO_4^0$, $CaPO_4^-$, and $H_2PO_4^-$. Substituting a mean river water composition

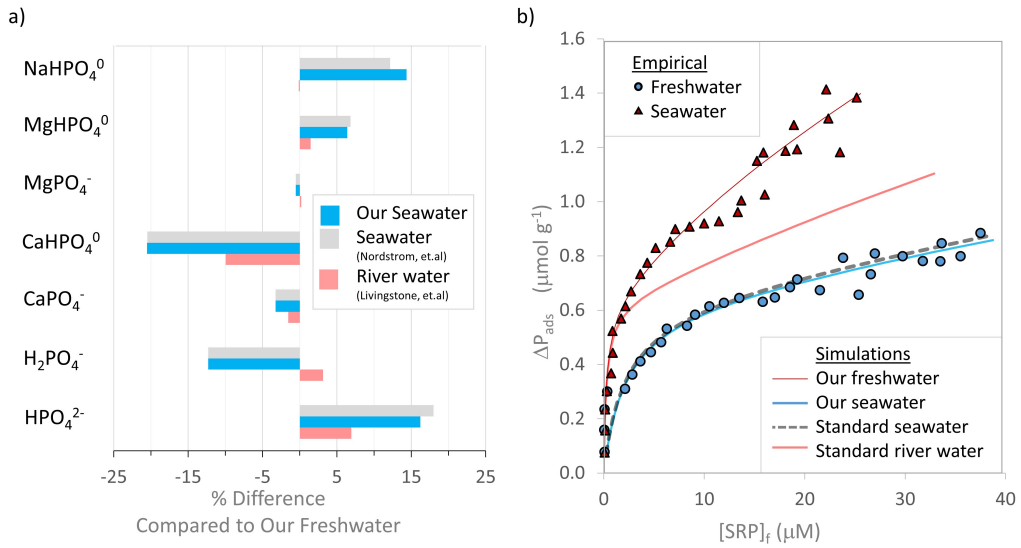

Figure 7 a) P speciation in our freshwater compared to our seawater, a reference seawater from Nordstrom et al. (1979) and a reference river water composition from Livingstone (1963), presented as % difference compared to aqueous P speciation in our freshwater; b) predicted P adsorption for these reference water types compared to the freshwater and seawater used in this study.

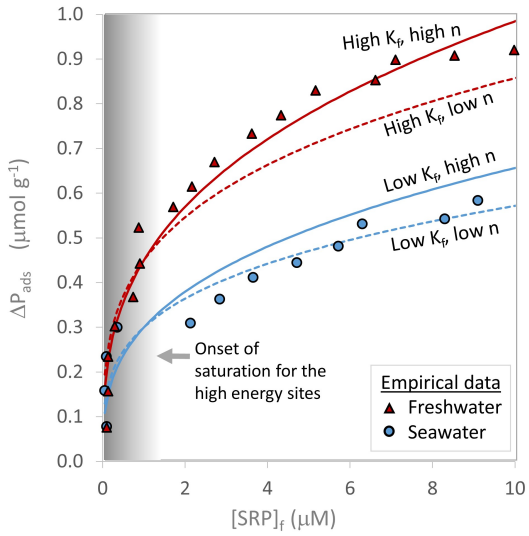

Figure 8 The influence of Freundlich isotherm parameters, shown with empirical data for reference (red triangles for freshwater, blue circles for seawater), where curves bearing the "High" freshwater K_f are red and those bearing the "Low" seawater K_f are blue, and those bearing the "high" freshwater n are shown as solid curves, and the "low" seawater n as dashed curves. Our hypothesized transition between the prominence of the first and second surfaces is shown as gray vs. white background.

from Livingstone (1963) in place of our freshwater solution produced a ΔP_{ads} curve that diverged from our freshwater curve to eventually become more intermediate between our freshwater and seawater curves (Figure 7b). There was negligible difference in ΔP_{ads} predicted for our seawater and the standard seawater.

5. Discussion

We developed the first (to our knowledge) geochemical models that simulates differential P adsorption to calcite in freshwater vs. seawater (Table 5, Figures 2a and 4). Our models build on existing surface complexation reactions in the CCM and adapts them for the natural complex electrolyte solutions (Pokrovsky and Schott, 1999; Pokrovsky et al., 1999; Sø et al., 2011).

507 The purpose of this study is to better understand the underlying mechanism for strong P
508 adsorption to calcite in freshwater by contrasting it with the same process in seawater. Our
509 results suggest that the preferential P species adsorbing at positively charged calcium sites on the
510 calcite surface differs depending on water type: $CaPO_4^-$ in freshwater and HPO_4^{2-} in seawater.
511 The adsorption of HPO_4^{2-} is consistent with a sorption edge study of P adsorption to sediments
512 from Taihu Lake, China (Zhou et al. (2005).
513 The surface reactions we used in our model (based on Sø et al. (2011)) are consistent
514 with longstanding scientific consensus that P adsorption is typically specific (i.e., inner sphere,
515 meaning that no water molecules are between the adsorption sites and the adsorbing anion) and
516 further that P adsorption occurs via ligand exchange with anions (in our case, mainly carbonate)
517 chemically bonded to metallic ions at the sorbent surface (in our case, calcium) (Goldberg and
518 Sposito, 1985). Ligand exchange is highly selective as to the anions and can remove large
519 proportions of anions even in quite dilute solutions with high concentrations of less selective
520 anions (Loganathan et al., 2014). Spectroscopic investigation of P adsorption to hematite have
521 supported the dominance of the inner sphere adsorption mechanism, while highlighting the
522 variability of complexes based on pH and surface coverage (Elzinga and Sparks, 2007). This
523 spectroscopic finding is consistent with our modeling observation that adsorbing P species alters
524 depending on water type. Although spectroscopy was beyond the scope of this study, in the
525 future it would be valuable to use spectroscopic techniques such as scanning electromicroscopy,
526 X-ray absorption fine structure and Fourier-Transform infrared analysis to further explore the
527 mechanism of P adsorption to calcite under a variety of water types and conditions.
528 Adsorption of P is sometimes accompanied by precipitation of calcium phosphate phases
529 such as apatite (e.g., $Ca_5(PO_4)_3(OH)$), although we have reason to believe this process was

530 negligible in our experiments. It is true that when aqueous P concentrations are much higher than
531 ours and pH is high, crystalline phases of apatite (e.g., $Ca_5(PO_4)_3(OH)$) can substantially enhance
532 removal of P from solution when the absorbent is calcium-enhanced biochar or calcite (Sø et al.,
533 2011; Loganathan et al., 2014; Wang et al., 2018). However, the low concentrations of aqueous
534 P and the lower pH of our experiments make apatite precipitation unlikely, based on parameters
535 outlined by Sø et al. (2011). Further, we conducted PHREEQC simulations of apatite
536 precipitation in the context of our experiments (shown and discussed in Appendix B), and found
537 that if precipitation had occurred, it would have occurred in certain of our seawater solutions and
538 none of our freshwater solutions. Such precipitation would have been measured as heightened P
539 removal (ΔP) in a few of our seawater solutions, whereas in our experiments much more P was
540 removed from our freshwater solutions (Figure 3). It is likely that the Mg^{2+} concentrations in our
541 seawater inhibited the precipitation of calcium-phosphate phases, as has been observed in other
542 studies (Salimi et al., 1985; Cao and Harris, 2008).
543 In Sections 5.1 and 5.2 below, we will discuss in detail further clues as to P dynamics at
544 the calcite surface, and in Section 5.3 we will present our conceptual model.
545
546 **5.1 Different adsorption sites at the calcite surface**
547 In calcite, as for soils, it is generally necessary to consider more than one type of
548 adsorption site (or "surface") with contrasting energies in order to adequately capture the
549 interactions between dissolved constituents and the solid surface (Wolthers et al., 2012). Despite
550 the array of different energies on the real calcite surface (described below), we found that
551 dividing adsorption sites into just two types of sites (strong and weak) was sufficient to fit our
552 empirical data well.

5.1.1 Microscopic calcite adsorption sites

Calcite crystal faces have different energy depending on whether they are terminated by both calcium and carbonate functional groups (low energy) or solely calcium or solely carbonate (high energy) (Sekkal and Zaoui, 2013). The dipole moment of polar faces makes them unstable, and adsorption of ions can neutralized the charge. Arguably the most important factors for determining calcite surface reactivity are corners and surface topography (Wolthers et al., 2012). Calcite crystals have perfect cleavage along rhombohedral planes in the crystal lattice, resulting in acute or obtuse angles where damage or other imperfections occur. The acute edges of stepped surfaces such as "etch pits" (depressions) and "islands" (plateaus) have much stronger charge than the obtuse angles.

5.1.2 High vs. low energy sites in our surface complexation model

Our simulations allow us to observe the shift as to which types of sites drive the greater P adsorption in both freshwater and seawater. Strong calcium sites drive P adsorption at low P concentrations (i.e., left-most side of graph, analogous to oligotrophic conditions) and weak calcium sites dominate at higher P concentration (above ~ 1-5 μM $[SRP]_f$, middle-to-right hand side of graphs, Figure 4c & d). The strong sites are effective at attracting P, but they soon approach saturation at elevated solution P concentrations (Figure 4c). At about the mid-point in Figure 4d, adsorption of P to weak calcium sites comes to dominate total P adsorption in freshwater, whereas in seawater weak calcium sites never reach more than 1/3 of the total P adsorption.

5.1.3 High vs. low energy sites in our Two-Surface Langmuir Isotherm

The strong and weak calcium sites in our computer model correspond to the "high energy" and "low energy" surfaces in the Two-Surface Langmuir Isotherm as described by

576 Holford et al. (1974) for soils. Like our thermodynamic model, the Langmuir Isotherm assumes
577 two types of adsorption sites with monolayer adsorption (no stacking of adsorbates) that have a
578 fixed number, and thus these sites can become saturated. The equation is derived from an
579 equilibrium-approach to P adsorption analogous to solubility reactions.

580 Thus, our Langmuir isotherm parameters for the two surfaces (P_{max1}, K_{eq1} for Surface 1,
581 and P_{max2} and K_{eq2} for Surface 2, Table 4) can be compared to strong vs. weak calcium sites on
582 the calcite surface in Figure 4. The Langmuir estimate of saturation concentration for the first
583 surface in freshwater (P_{max1} = 0.68 μmol P g^{-1}) matches the corresponding value from our
584 computer simulation (0.612 μmol P g^{-1}), estimated using the end point of the flattened solid red
585 curve in Figure 4c. For seawater the match is not as good; the computer simulated saturation
586 (0.588 μmol P g^{-1}) is double the Langmuir estimate (0.24 μmol P g^{-1}), and we will argue that this
587 can be explained by the role of P_{max} in determining the shape of the isotherms. (We were not able
588 to use our computer simulation to estimate a saturation concentration since the trend of P
589 adsorption to weak calcium sites is linear, shown as dashed lines in Figure 4c).

590 We find that in our Langmuir isotherms, relative saturation concentrations (P_{max1} and
591 P_{max2} for freshwater vs. seawater) drive their differences in ΔP_{ads}, and not the other parameters
592 (K_{eq1} and K_{eq2}). The saturation concentration at the first surface is almost three times higher in
593 freshwater vs. seawater, and at the second surface it's almost a factor of 5 (Table 4). In contrast,
594 the relative binding energies (K_{eq1} and K_{eq2}, also described as the affinity of P for the surface) are
595 actually higher in seawater at both types of sites. These findings are consistent with a batch study
596 of P adsorption to calcareous sediment in freshwater and seawater (Flower et al., 2016).

597 Further, since the solid material was the same for all of our experiments, the observed
598 differences in saturation concentrations (P_{max1} and P_{max2}) between our freshwater and seawater

599 data do not reflect the intrinsic adsorption site concentrations (although they would in studies
600 comparing different sediments). Instead, differences in these parameters in the present study
601 reflect the influence of water quality on the availability to P of adsorption sites on the calcite
602 surface, by altering the concentrations of the preferred adsorbing P species, as well as the ability
603 of P to compete with other ions for adsorption sites, and perhaps also altering kinetic factors.
604
605 ***5.1.4 High vs. low energy sites in our Freundlich Isotherm***
606 Like the Langmuir isotherm, the Freundlich isotherm [Equation 4] is also considered a
607 good choice for heterogeneous surfaces, and it fits well with a wide range of adsorption data for
608 minerals and soils. The Freundlich isotherm differs from the Langmuir in two key ways: (1) it
609 assumes that the solid surface does not become saturated, since a power function with a
610 fractional exponent does not converge, and thus does not have an upper limit or saturation
611 concentration, and (2) it is empirically based, in contrast the theoretical basis of the Langmuir
612 isotherm.
613 The influence of K_f, the coefficient of the power function, is most prominent in
614 determining the initial steepness of the curve at low P concentrations (the left hand side of the
615 graph). Plots of curves with the same K_f value (red vs. blue curves in Figure 8) initially produce
616 nearly the same ΔP_{ads} regardless whether the n was the freshwater value (solid curves) or the
617 seawater value (dashed curves). Thus, K_f reflects the initial prominence of intense P adsorption
618 at the first surface (the strong sites), closely relating it to P_{max1} in the Langmuir Two-Surface
619 Isotherm, and the strong sites in our computer simulation (Figure 4a and b). The Freundlich K_f
620 has been described as the relative adsorption capacity, or the relative rate of removal of
621 phosphorus per unit increase in $[SRP]_f$ (Yakubu et al., 2008).

There is a clear point when the influence of the Freundlich exponent n causes curves with the same K_f to diverge. The point of divergence may roughly reflect the increasing importance of the second, lower energy surface, due to the first surface starting to become saturated. The lower the fractional exponent n, the shallower the slope in the subsequent part of the curve. Although the Freundlich exponent n has been described as representing the bond strength between P and the surface (Yakubu et al., 2008), this interpretation may be most relevant when comparing the P adsorption to solids with different characteristics. For our experimental data, the fractional exponent n closely relates to the diminished site availability for P at the lower energy surface, corresponding to (P_{max1}) of the Langmuir Two-Surface Isotherm.

5.1.5 Three ways to model high vs. low energy sites on calcite

In the preceding sections we have shown that P dynamics at the heterogeneous calcite surface are accounted for with distinct parameters for the high vs. low energy adsorption sites in our three different approaches to predicting/ describing P adsorption to calcite, and that all of these are higher in freshwater vs. seawater (Tables 4 & 5). This allows us to draw connections between these heretofore disparate systems, shown in Table 6).

Table 6 Our conceptual model of how the heterogeneity of the calcite surface is accounted for in the various approaches to predicting/describing P adsorption. All of these six parameters are higher in freshwater compared to seawater in this study.

	High energy sites	**Low energy sites**
Surface complexation Model	Log K for P adsorption at $>sCa^+$	Log K for P adsorption at $>wCa^+$
Langmuir Two-Surface Isotherm	P_{max1}	P_{max2}
Freundlich Isotherm	K_f	n

644 **5.2 Solution composition: effects on surface charge and P adsorption**

645 Dissolved ions in solution can also trigger differential behavior of P at the calcite surface
646 in seawater vs. freshwater. In a study of electrokinetics at the solid-solution interface of calcite
647 Mahani et al. (2017) measured the ζ-potential at the surface of different types of carbonate rock
648 immersed in a variety of chemical solutions. They found the divalent ions Ca^{2+} and CO_3^{2-} to be
649 the most important for determining calcite surface charge, dubbing them the "potential-
650 determining ions" (Mahani et al., 2017). The monovalent ions and H^+ and OH^- are secondary due
651 to their lower concentrations in seawater compared to the major seawater ions, while Na^+ and K^+
652 were found to have little or no effect on calcite surface properties, suggesting little adsorption to
653 the surface (Mahani et al., 2017).

654 The effect of increasing concentrations of Ca^{2+} and Mg^{2+} in solution is to make the calcite
655 surface increasingly positive (Zhang and Austad, 2006; Mahani et al., 2017). In batch
656 experiments, Millero et al. (2001) found that these cations enhanced P adsorption when added to
657 NaCl solutions. They suggested that Ca^{2+} and Mg^{2+} facilitate P adsorption through bridged
658 reactions, or through the adsorption of Ca^{2+}-P or Mg^{2+}-P ion pairs. Our scenarios indicate
659 enhanced P adsorption with increased Ca^{2+} concentration (Figure 6a and b). Doubling
660 concentration of Ca^{2+} in the initial seawater solution strongly enhanced ΔP_{ads} (by up to 16%);
661 and omitting these ions in the initial seawater solution decreased ΔP_{ads} (by up to 22%). Since
662 HPO_4^{2-} is the sole adsorbing P species in our seawater model, it is not clear how Ca^{2+} enhances P
663 adsorption within that model.

664 Conversely, Mg^{2+} has the opposite effect: doubling Mg^{2+} ions in our initial seawater
665 solution diminished ΔP_{ads} by 9%, and omitting them increased the ΔP_{ads} by up to 22%. (Figure 6a
666 and b). We were not able to develop a successful model involving the adsorption of Mg^{2+}-P ion

667 pairs. The role of seawater Mg^{2+} and Na^{+} in our simulations is to strongly inhibit P adsorption by
668 forming aqueous complexes with P. Compared to our freshwater, our seawater has much more
669 $MgHPO_4^0$, $NaHPO_4^0$, and HPO_4^{2-}, and much less $CaHPO_4^0$, $CaPO_4^-$, and $H_2PO_4^-$ (Figure 7a). The
670 change in P speciation causes HPO_4^{2-} to be the preferred adsorbing P species in seawater, as
671 opposed to $CaPO_4^-$ in freshwater. The greater availability of $CaPO_4^-$ to adsorb to calcite in
672 freshwater due to lower concentrations of Mg^{2+} and Na^{+} may be a key driver of increased P
673 adsorption in freshwater vs. seawater.
674 Although less has been said in the literature about Na^{+} inhibiting P adsorption, there is
675 longstanding support in the literature for Mg^{2+} ions decreasing P adsorption by forming Mg^{2+}-P
676 ion pairs, thereby inhibiting the formation of Ca^{2+}-P ion pairs that might otherwise adsorb to the
677 surface (Leckie and Stumm, 1970; Kitano et al., 1978; Kuo and Mikkelsen, 1979; Yadav et al.,
678 1984; Shariatmadari and Mermut, 1999). The influence of Mg^{2+} does not have to do with its
679 interactions at the calcite surface in our model. Even though Mg^{2+} fills 76% of the carbonate
680 sites in seawater (Figure 4c), removing the Mg^{2+} surface complex ($>CO_3Mg^{+}$) from the script did
681 not make much difference in the predicted ΔP_{ads} (Figure 6a).
682 Oxyanions can inhibit P adsorption through an alternative route. Divalent anions like
683 SO_4^{2-} make the surface more negatively charged (Zhang and Austad, 2006). In batch studies with
684 aragonite (a polymorph of calcite) in NaCl solutions, the tendency of Ca^{2+} and Mg^{2+} to enhance
685 P adsorption to aragonite was diminished with the addition of SO_4^{2-}, or CO_3^{2-}/ HCO_3^- at seawater
686 strength (Millero et al., 2001). Millero et al. (2001) proposed that HCO_3^- was the primary driver
687 of diminished P adsorption to aragonite in seawater. In two different studies using batch
688 experiments with low salinity solutions, an increase in HCO_3^- concentration resulted in a
689 decrease in P adsorption to $CaCO_3$ (Millero et al., 2001; Sø et al., 2011). Further, in batch studies

690 with aragonite in solutions across a range of salinities, P adsorption remained nearly the same
691 when HCO_3^- concentration was held constant (at 2 mM) (Millero et al., 2001).
692 Based on these observations, Millero et al. (2001) predicted that if freshwater in a given
693 region had higher HCO_3^- concentrations than seawater, less P would absorb to sediment particles
694 in such freshwater compared to seawater. Flower et al. (2016) supported this hypothesis when
695 they reported less P adsorption to calcareous sediment when immersed in a brackish groundwater
696 with unusually high total alkalinity (presumed to mainly consist of HCO_3^-/CO_3^{2-}) vs. when
697 immersed in full strength natural seawater with lower total alkalinity. However, the experiments
698 in the present study do not support the hypothesis that higher total alkalinity *per se* is a primary
699 driver of diminished P adsorption in seawater vs. freshwater. Despite the fact that total alkalinity
700 was higher in our freshwater solution compared to our seawater (Table 1), our freshwater
701 solutions still produced markedly higher P adsorption than our seawater solutions (Figure 3a). In
702 freshwater (compared to seawater) calcite exhibited higher adsorption capacity (K_f), higher bond
703 strength (n), higher saturation concentrations (P_{max1} and P_{max2}), and higher Log K's (Tables 2 &
704 3). When we simulated double total alkalinity in our initial seawater solution, this only very
705 slightly reduced predicted ΔP_{ads}, and omitting initial seawater total alkalinity altogether only
706 slightly increased predicted ΔP_{ads} (Figure 6a).
707 Even when CO_3^{2-} concentrations are low, these ions still cause more P to adsorb in
708 freshwater compared to seawater. The distribution of surface complexes (Figure 5) shows that
709 even though our freshwater has 22% higher total alkalinity (Table 1), the calcite surface has 40
710 times less CO_3^{2-} adsorbed at strong calcium sites in freshwater compared to seawater, and only a
711 quarter of the CO_3^{2-} adsorbed at weak calcium sites. An obscure aspect of the thermodynamics of

712 the seawater solution appears to enhance the competitive edge of CO_3^{2-} against P at both types of
713 calcium sites.

714 It is worth noting that CO_3^{2-} domination of the weak calcium sites in seawater occurs
715 despite the fact that HCO_3^- is the much more abundant dissolved carbonate species at the pH we
716 used for both our solutions (pH = 7.7). Although our model includes surface reactions for HCO_3^-
717 at both strong and weak calcium sites (Table 3), HCO_3^- never adsorbs to more than 0.4% of
718 strong calcium sites, or 4% of weak calcium sites. Pokrovsky and Schott (2002) determined that
719 the Log K for HCO_3^- substituting for CO_3^{2-} at calcium sites was quite low (-3.929), strongly
720 favoring the CO_3^{2-} (Table 3). A recent study has shown that CO_3^{2-} can be the dominant species of
721 inorganic carbon at the calcite surface even when HCO_3^- is the dominant species in the solution
722 (i.e., 7.5 < pH <10.35) (Andersson et al., 2016).

723 Sulfate does not appear to influence ΔP_{ads} in our simulations. We saw no change in the
724 predicted ΔP_{ads} when we doubled or eliminated SO_4^{2-} ions in the initial seawater solution, nor
725 when we omitted the sulfate surface reaction (Figure 5a). It's interesting to note that sulfate
726 occupied on weak calcium sites is four times more in freshwater than that in seawater (Figure 5),
727 despite the fact that seawater has six times more sulfate than the freshwater (Table 1).
728 Apparently, seawater chemistry allows CO_3^{2-} to outcompete SO_4^{2-} as well as P at weak sites. The
729 accumulating literature that shows SO_4^{2-} as a driver of diminished P adsorption involves soils
730 undergoing microbially mediated sulfate reduction and the formation of iron sulfides (Caraco et
731 al., 1989; Roden and Edmonds, 1997; Lamers et al., 1998; Lucassen et al., 2004; Zak et al.,
732 2006). There is little if any evidence in literature for an abiotic process whereby SO_4^{2-} drives
733 diminished P adsorption.

734 **5.3 The mechanism for strong P adsorption in Freshwater**

735 As laid out in Sections 5.1 and 5.2, the significantly greater ΔP_{ads} in freshwater vs.
736 seawater appears to be driven mainly by three factors:
737
738 1) The adsorbing P species in freshwater ($CaPO_4^-$) is more thermodynamically favorable than
739 the adsorbing P species in seawater (HPO_4^{2-}) (Table 3).
740 2) Freshwater has high concentrations $CaPO_4^-$ (Figure 7a). In seawater, the high concentrations
741 of Na^+ and Mg^{2+} drive aqueous P speciation to $NaHPO_4^0$ and $MgHPO_4^0$, which may
742 scavenge P from the surface, and also makes $CaPO_4^-$ too scarce to adsorb in appreciable
743 amounts (Figure 7).
744 3) P more effectively competes with CO_3^{2-} for adsorption sites at the calcite surface in
745 freshwater, even when the CO_3^{2-} concentration is high. In seawater, CO_3^{2-} ions outcompete
746 all other ions (i.e., HPO_4^{2-}, SO_4^{2-}, and H_2O) at weak calcium sites (Figure 5). The enhanced
747 favorability of CO_3^{2-} surface complexes in seawater is due to the thermodynamics of
748 seawater chemistry.
749
750 If a main driver of stronger P adsorption in freshwater vs. seawater arises more from the aqueous
751 chemistry than specific surface reactions, this may help explain why the phenomenon is nearly
752 ubiquitous globally, across wide-ranging lithologies.
753
754 **5.4 Limitations**
755 Any model is a simplification of the real world, and one must understand it and apply it
756 within its limitations. The fact that our model fits the data well does not mean that its explanation
757 is correct, only that it is internally consistent between our laboratory measurements and

published thermodynamic data for relevant components of the system, within the code that we used. Some of the limitations in our study include that we focused our experiments on the influence of water composition between freshwater and seawater under benchtop (oxic) conditions with biological activity suppressed (with chloroform). We also recognize that myriad physicochemical factors influence P adsorption capacity, such as pH and redox (Pant and Reddy, 2001; McDonald et al., 2019). Second, we employed many simplifying assumptions in order to code our model. For example, we made assumptions about the nature of the calcite surface, including that P adsorbs to calcium sites (rather than carbonate sites), and that there are two main types of calcium sites (strong and weak).

6. Conclusions

The strength of P adsorption to soils and sediments in freshwater drives P limitation in many freshwater aquatic systems (Paludan and Morris, 1999; Vitousek et al., 2010). The high capacity of sediment to adsorb P in freshwater also has important implications for coastal areas, because suspended sediment with adsorbed P is transported to estuaries where contact with seawater causes it to be released (Froelich, 1988). The process of P adsorption has also proven important in a variety of decontamination efforts such as sewage remediation and the extraction of pollutants such as uranium from wastewater (Kong et al., 2020). This paper demonstrates how geochemical thermodynamic simulations can be used to develop complexation models that can help explain differential P adsorption to calcite in seawater vs. freshwater. Our surface complexation model for P adsorption to calcite in freshwater and seawater is an important step forward in predicting the role that sediment can play in the coming decades, as freshwater areas become increasingly polluted with P, and sea level rise brings increasing seawater into

781 previously freshwater regions. The model provided in this study could be used as a basis for
782 modeling P remediation in freshwater and seawater field conditions, as well as the fate of P
783 adsorbed in freshwater and estuarine wetlands.

784 Acknowledgements

785 We appreciate Annie Majette, Paulina Ramirez, Andre Rives, and William Westerfield for
786 laboratory support, Cody Stephens for coding support, Dr. Eloy Martinez for providing
787 laboratory equipment, and we are grateful to the Rains Ecohydrology Lab group at USF Tampa,
788 especially Leanne Stepchinski and Dr. Kai Rains, for editorial comments, and Dr. Scott
789 Campbell for recruiting interns. This manuscript has benefited from the thoughtful comments of
790 reviewers. The scientific results and conclusions, as well as any views or opinions expressed
791 herein, are those of the authors and do not necessarily reflect the views of NOAA or the
792 Department of Commerce. This material is based upon work supported by the National Science
793 Foundation through the Florida Coastal Everglades Long-Term Ecological Research program
794 under Cooperative Agreements #DEB-1237517, #DBI-0620409, and #DEB-9910514. This is
795 contribution number _____ from the Southeast
796 Environmental Research Center in the Institute of Water & Environment at Florida International
797 University.

798

799 References

800 Andersson, M.P., Rodriguez-Blanco, J., Stipp, S.L.S., 2016. Is bicarbonate stable in and on the
801 calcite surface? Geochim. Cosmochim. Acta 176, 198-205.
802 Brandano, M., Frezza, V., Tomassetti, L., Cuffaro, M., 2009. Heterozoan carbonates in
803 oligotrophic tropical waters: the Attard member of the lower coralline limestone
804 formation (Upper Oligocene, Malta). Palaeogeogr. Palaeoclimatol. Palaeoecol. 274, 54-
805 63.

Cao, X., Harris, W., 2008. Carbonate and magnesium interactive effect on calcium phosphate precipitation. Environ. Sci. Technol. 42, 436-442.
Caraco, N., Cole, J., Likens, G., 1989. Evidence for sulphate-controlled phosphorus release from sediments of aquatic systems.
D'Angelo, E., Crutchfield, J., Vandiviere, M., 2001. Rapid, sensitive, microscale determination of phosphate in water and soil. J. Environ. Qual. 30, 2206-2209.
de Kanel, J., Morse, J.W., 1978. The chemistry of orthophosphate uptake from seawater on to calcite and aragonite. Geochim. Cosmochim. Acta 42, 1335-1340.
Detenbeck, N.E., Brezonik, P.L., 1991. Phosphorus sorption by sediments from a soft-water seepage lake. 1. An evaluation of kinetic and equilibrium models. Environ. Sci. Technol. 25, 395-403.
Doherty, J., 2004. PEST model-independent parameter estimation user manual. Watermark Numerical Computing, Brisbane, Australia 3338, 3349.
Dzombak, D.A., Morel, F.M., 1990. Surface complexation modeling: hydrous ferric oxide. John Wiley & Sons.
Elzinga, E.J., Sparks, D.L., 2007. Phosphate adsorption onto hematite: An in situ ATR-FTIR investigation of the effects of pH and loading level on the mode of phosphate surface complexation. Journal of Colloid and Interface Science 308, 53-70.
Fetter, C., 1977. Attenuation of waste water elutriated through glacial outwash. Groundwater 15, 365-371.
Filippelli, G.M., 2008. The global phosphorus cycle: past, present, and future. Elements 4, 89-95.
Flower, H., Rains, M., Lewis, D., Zhang, J.-Z., Price, R., 2016. Control of phosphorus concentration through adsorption and desorption in shallow groundwater of subtropical carbonate estuary. Estuar. Coast. Shelf Sci. 169, 238-247.
Freundlich, H., 1906. Freundlich's Adsorption Isotherm. Phys. Chem 57, 384.
Froelich, P.N., 1988. Kinetic control of dissolved phosphate in natural rivers and estuaries: A primer on the phosphate buffer mechanism1. Limnol. Oceanogr. 33, 649-668.
Gao, Y., Mucci, A., 2003. Individual and competitive adsorption of phosphate and arsenate on goethite in artificial seawater. Chem. Geol. 199, 91-109.
Garing, C., Luquot, L., Pezard, P., Gouze, P., 2013. Geochemical investigations of saltwater intrusion into the coastal carbonate aquifer of Mallorca, Spain. J. Appl. Geochem. 39, 1-10.
Goldberg, S., Criscenti, L.J., Turner, D.R., Davis, J.A., Cantrell, K.J., 2007. Adsorption–desorption processes in subsurface reactive transport modeling. Vadose Zone J. 6, 407-435.
Goldberg, S., Sposito, G., 1985. On the mechanism of specific phosphate adsorption by hydroxylated mineral surfaces: A review. Communications in Soil Science & Plant Analysis 16, 801-821.
Hiorth, A., Cathles, L., Madland, M., 2010. The impact of pore water chemistry on carbonate surface charge and oil wettability. Transp Porous Media. 85, 1-21.
Holford, I., Wedderburn, R., Mattingly, G., 1974. A Langmuir two-surface equation as a model for phosphate adsorption by soils. J. Soil Sci. 25, 242-255.
Hou, E., Luo, Y., Kuang, Y., Chen, C., Lu, X., Jiang, L., Luo, X., Wen, D., 2020. Global meta-analysis shows pervasive phosphorus limitation of aboveground plant production in natural terrestrial ecosystems. Nat. Commun. 11, 1-9.

Kitano, Y., Okumura, M., Idogaki, M., 1978. Uptake of phosphate ions by calcium carbonate. Geochem. J. 12, 29-37.
Kogure, T., Aoki, H., Maekado, A., Hirose, T., Matsukura, Y., 2006. Effect of the development of notches and tension cracks on instability of limestone coastal cliffs in the Ryukyus, Japan. Geomorphology 80, 236-244.
Kong, L., Ruan, Y., Zheng, Q., Su, M., Diao, Z., Chen, D., Hou, L.a., Chang, X., Shih, K., 2020. Uranium extraction using hydroxyapatite recovered from phosphorus containing wastewater. Journal of hazardous materials 382, 120784.
Kuo, S., Mikkelsen, D., 1979. Effect of Magnesium on Phosphate Adsorption by Calcium Carbonate. Soil Sci. 127, 65-69.
Lamers, L.P., Tomassen, H.B., Roelofs, J.G., 1998. Sulfate-induced eutrophication and phytotoxicity in freshwater wetlands. Environ. Sci. Technol. 32, 199-205.
Langmuir, D., 1968. Stability of calcite based on aqueous solubility measurements. Geochimica et Cosmochimica Acta 32, 835-851.
Langmuir, I., 1918. The adsorption of gases on plane surfaces of glass, mica and platinum. J. Am. Chem. Soc. 40, 1361-1403.
Leckie, J.O., Stumm, W., 1970. Phosphate precipitation. Water Resources Symposium 3, 237-249.
Lee, S.S., Heberling, F., Sturchio, N.C., Eng, P.J., Fenter, P., 2016. Surface Charge of the Calcite (104) Terrace Measured by Rb+ Adsorption in Aqueous Solutions Using Resonant Anomalous X-ray Reflectivity. The Journal of Physical Chemistry C.
Livingstone, D.A., 1963. Chemical composition of rivers and lakes. US Government Printing Office.
Loganathan, P., Vigneswaran, S., Kandasamy, J., Bolan, N.S., 2014. Removal and recovery of phosphate from water using sorption. Critical Reviews in Environmental Science and Technology 44, 847-907.
Lucassen, E., P Smolders, A., Van de Crommenacker, J., Roelofs, J., 2004. Effects of stagnating sulphate-rich groundwater on the mobility of phosphate in freshwater wetlands: a field experiment. Archiv für hydrobiologie 160, 117-131.
Mahani, H., Keya, A.L., Berg, S., Nasralla, R., 2017. Electrokinetics of carbonate/brine interface in low-salinity waterflooding: Effect of brine salinity, composition, rock type, and pH on ζ-potential and a surface-complexation model. Spe Journal 22, 53-68.
McDonald, G.J., Norton, S.A., Fernandez, I.J., Hoppe, K.M., Dennis, J., Amirbahman, A., 2019. Chemical controls on dissolved phosphorus mobilization in a calcareous agricultural stream during base flow. Science of The Total Environment 660, 876-885.
Millero, F., Huang, F., Zhu, X., Liu, X., Zhang, J.-Z., 2001. Adsorption and desorption of phosphate on calcite and aragonite in seawater. Aquat. Geochem. 7, 33-56.
Millero, F.J., Schreiber, D., 1982. Use of the ion pairing model to estimate activity coefficients of the ionic components of natural waters. Am. J. Sci. 282, 1508-1540.
Morse, J.W., Mucci, A., Millero, F.J., 1980. The solubility of calcite and aragonite in seawater of 35%. salinity at 25 C and atmospheric pressure. Geochim. Cosmochim. Acta 44, 85-94.
Morse, J.W., Zullig, J.J., Bernstein, L.D., Millero, F.J., Milne, P., Mucci, A., Choppin, G.R., 1985. Chemistry of calcium carbonate-rich shallow water sediments in the Bahamas. J Am. J. Sci. 285.

Nordstrom, D., Plummer, L., Wigley, T., Wolery, T., Ball, J.W., Jenne, E., Bassett, R., Crerar, D., Florence, T., Fritz, B., 1979. A comparison of computerized chemical models for equilibrium calculations in aqueous systems. in: Jenne, E.A. (Ed.). Chemical Modeling in aqueous systems, speciation, sorption, solubility, and kinetics. ACS Publications, pp. 857-892.

Paludan, C., Morris, J.T., 1999. Distribution and speciation of phosphorus along a salinity gradient in intertidal marsh sediments. Biogeochemistry 45, 197-221.

Pant, H., Reddy, K., 2001. Phosphorus sorption characteristics of estuarine sediments under different redox conditions. J. Environ. Qual. 30, 1474-1480.

Parkhurst, D.L., Appelo, C., 2013. Description of input and examples for PHREEQC version 3: a computer program for speciation, batch-reaction, one-dimensional transport, and inverse geochemical calculations U.S. Geological Survey Techniques and Methods No. 6-A43. US Geological Survey.

Parkhurst, D.L., Appelo, C.J.W.-r.i.r., 1999. User's guide to PHREEQC (version 2)–a computer program for speciation, batch-reaction, one-dimensional transport, and inverse geochemical calculations. 99, 312.

Pierrot, D., Millero, F.J., 2016. The Speciation of Metals in Natural Waters. Aquat. Geochem., 1-20.

Plummer, L.N., Busenberg, E., 1982. The solubilities of calcite, aragonite and vaterite in CO2-H2O solutions between 0 and 90 C, and an evaluation of the aqueous model for the system CaCO3-CO2-H2O. Geochimica et cosmochimica acta 46, 1011-1040.

Pokrovsky, O., Mielczarski, J., Barres, O., Schott, J., 2000. Surface speciation models of calcite and dolomite/aqueous solution interfaces and their spectroscopic evaluation. Langmuir 16, 2677-2688.

Pokrovsky, O., Schott, J., 2002. Surface chemistry and dissolution kinetics of divalent metal carbonates. Environ. Sci. Technol. 36, 426-432.

Pokrovsky, O.S., Schott, J., 1999. Processes at the magnesium-bearing carbonates/solution interface. II. Kinetics and mechanism of magnesite dissolution. Geochimica et cosmochimica acta 63, 881-897.

Pokrovsky, O.S., Schott, J., Thomas, F., 1999. Dolomite surface speciation and reactivity in aquatic systems. Geochimica et Cosmochimica Acta 63, 3133-3143.

Prastka, K., Sanders, R., Jickells, T., 1998. Has the role of estuaries as sources or sinks of dissolved inorganic phosphorus changed over time? Results of a Kd study. Mar. Pollut. Bull. 36, 718-728.

Reddy, K., Graetz, D., 1981. Use of shallow reservoir and flooded organic soil systems for waste water treatment: nitrogen and phosphorus transformations. Journal of Environmental Quality 10, 113-119.

Richardson, C.J., 1985. Mechanisms controlling phosphorus retention capacity in freshwater wetlands. Science 228, 1424-1427.

Riemersma, S., Little, J., Ontkean, G., Moskal-Hébert, T., 2006. Phosphorus sources and sinks in watersheds: A review. 82 pp. Alberta soil phosphorus limits project 5.

Roden, E., Edmonds, J., 1997. Phosphate mobilization in iron-rich anaerobic sediments: microbial Fe (III) oxide reduction versus iron-sulfide formation. Archiv für Hydrobiologie 139, 347-378.

939 Salimi, M., Heughebaert, J., Nancollas, G., 1985. Crystal growth of calcium phosphates in the
940 presence of magnesium ions. Langmuir 1, 119-122.
941 Sekkal, W., Zaoui, A., 2013. Nanoscale analysis of the morphology and surface stability of
942 calcium carbonate polymorphs. Sci. rep. 3.
943 Shariatmadari, H., Mermut, A., 1999. Magnesium-and silicon-induced phosphate desorption in
944 smectite–, palygorskite–, and sepiolite–calcite systems. Soil Sci Soc Am J 63, 1167-1173.
945 Shinn, E., 1973. Carbonate coastal accretion in an area of longshore transport, NE Qatar, Persian
946 Gulf. The Persian Gulf. Springer, pp. 179-191.
947 Sø, H.U., Postma, D., Jakobsen, R., Larsen, F., 2008. Sorption and desorption of arsenate and
948 arsenite on calcite. Geochim. Cosmochim. Acta 72, 5871-5884.
949 Sø, H.U., Postma, D., Jakobsen, R., Larsen, F., 2011. Sorption of phosphate onto calcite; results
950 from batch experiments and surface complexation modeling. Geochim. Cosmochim. Acta
951 75, 2911-2923.
952 Syers, J., Browman, M., Smillie, G., Corey, R., 1973. Phosphate sorption by soils evaluated by
953 the Langmuir adsorption equation. Soil Sci Soc Am J 37, 358-363.
954 Van Cappellen, P., Charlet, L., Stumm, W., Wersin, P., 1993. A surface complexation model of
955 the carbonate mineral-aqueous solution interface. Geochim. Cosmochim. Acta 57, 3505-
956 3518.
957 Vitousek, P.M., Porder, S., Houlton, B.Z., Chadwick, O.A., 2010. Terrestrial phosphorus
958 limitation: mechanisms, implications, and nitrogen–phosphorus interactions. Ecol Appl
959 20, 5-15.
960 Wang, S., Kong, L., Long, J., Su, M., Diao, Z., Chang, X., Chen, D., Song, G., Shih, K., 2018.
961 Adsorption of phosphorus by calcium-flour biochar: Isotherm, kinetic and transformation
962 studies. Chemosphere 195, 666-672.
963 Wolthers, M., Di Tommaso, D., Du, Z., de Leeuw, N., 2012. Calcite surface structure and
964 reactivity: molecular dynamics simulations and macroscopic surface modelling of the
965 calcite–water interface. Phys. Chem. Chem. Phys. 14, 15145-15157.
966 Yadav, B., Paliwal, K., Nimgade, N., 1984. Effect of magnesium-rich waters on phosphate
967 adsorption by calcite. Soil Sci. 138, 153-157.
968 Yakubu, M., Gumel, M., Abdullahi, A., 2008. Use of activated carbon from date seeds to treat
969 textile and tannery effluents. African Journal of Science and Technology (AJST) Science
970 and Engineering Series 9, 39-49.
971 Zak, D., Kleeberg, A., Hupfer, M., 2006. Sulphate-mediated phosphorus mobilization in riverine
972 sediments at increasing sulphate concentration, River Spree, NE Germany.
973 Biogeochemistry 80, 109-119.
974 Zhang, J.-Z., Huang, X.-L., 2011. Effect of temperature and salinity on phosphate sorption on
975 marine sediments. Environ. Sci. Technol. 45, 6831-6837.
976 Zhang, P., Austad, T., 2006. Wettability and oil recovery from carbonates: Effects of temperature
977 and potential determining ions. Colloids Surf. A Physicochem. Eng. Asp. 279, 179-187.
978 Zhou, A., Tang, H., Wang, D., 2005. Phosphorus adsorption on natural sediments: Modeling and
979 effects of pH and sediment composition. Water Res. 39, 1245-1254.
980 Zhou, M., Li, Y., 2001. Phosphorus-sorption characteristics of calcareous soils and limestone
981 from the southern Everglades and adjacent farmlands. Soil Sci Soc Am J 65, 1404-1412.

982